Corundum-type tubular and rod-like In_2O_3 nanocrystals: synthesis from designed InOOH and application in photocatalysis†

Li-Yong Chen, Zhen-Xiang Wang and Zu-De Zhang*

Received (in Gainesville, FL, USA) 7th October 2008, Accepted 22nd January 2009
First published as an Advance Article on the web 6th March 2009
DOI: 10.1039/b817588h

Indium oxyhydroxide (InOOH) 1-D nanostructures have been synthesized utilizing the hexamethylene diamine (HMDA)-assisted hydrolysis of In^{3+} cation method in the solvent poly(ethylene glycol 400) (PEG-400). It was found that the amount of distilled water and the solvent type were two key factors for the synthesis of high quality nanocrystals. The anisotropic growth of InOOH could be attributed to the HMDA molecule-assisted oriented attachment of nanoparticles, and the formation of tubular InOOH nanostructures could be due to "dissolution and recrystallization". By annealing InOOH precursors at 400 °C in air, hexagonal corundum-type indium sesquioxide (H-In_2O_3), which inherits the morphologies of its precursor with a slight size shrinking, was also prepared. The photocatalytic properties of tubular and rod-like H-In_2O_3 nanocrystals were investigated by the photodegradation of rhodamine B (RhB) molecules under ultraviolet (UV) light irradiation.

Introduction

Nanostructured materials have gained a steadily growing interest as a result of their peculiar and fascinating properties, and possible applications superior to their bulk counterparts.[1] In the past few years, much effort has been devoted to investigating shape-controlled low-dimensional nanomaterials, which have been considered as a broad perspective.[2] Among low-dimensional nanomaterials, 1-D nanomaterials have become a class of attractive materials for scientific and technological applications due to their unique chemical and physical properties, which can be attributed to their dimensional anisotropy.[3] In particular, 1-D nanomaterials with tubular structures, such as polymers, metals, metal oxides and ceramics,[4] have been successfully synthesized by various methods since the discovery of the carbon nanotube. The synthesis of tubular structures is an exciting field, owing to its specific structures, which have walls of nanometer thickness, interesting properties that differ from their solid counterparts and widespread potential applications in various fields, including lightweight materials, host materials, electrochemical devices, pollutant decomposition and sensors.[5] Tubular structures provide both chemical functionality and a designable inner space for meeting new technological challenges.

In the past decade, owing to their important physical and chemical properties, semiconductor metal oxides, with their special microstructures and nanoscale sizes, have attracted much attention in the field of material science. As a type of metal oxide, indium sesquioxide (In_2O_3), existing in cubic bixbyite-type and hexagonal corundum-type forms, has been found to be an important n-type semiconductor material with a direct band gap of 3.55–3.75 eV. The possible applications of nanostructured In_2O_3 in UV-vis lasers, detectors and gas sensors are extremely attractive.[6] Although In_2O_3 has been investigated and used for several decades, most In_2O_3 nanocrystals, having various morphologies, are in the form of a cubic bixbiyite-type structure. Few studies on the preparation and properties of metastable hexagonal In_2O_3 (H-In_2O_3) nanocrystals with a corundum-type structure by high-pressure modification have been reported. More recently, some notable work has appeared on the preparation of H-In_2O_3.[7] However, the synthesis of tubular H-In_2O_3 structures with a narrow diameter and uniform geometry have seldom been reported, except for a prominent work where tubular H-In_2O_3 nanocrystals were successfully prepared.[7e]

Poly(ethylene glycol) (PEG) molecules have been widely used in the synthesis of micro/nanomaterials with different shapes, for example WO_3 films,[8] CeO_2 nanorods[9] and α-NiS flower-like architectures.[10] PEG-400, a low molecular weight polymer, should also be a reasonable solvent due to its relatively high boiling point, non-toxicity and cheapness. Herein, the fabrication of tubular and rod-like H-In_2O_3 nanostructures is introduced through a facile two-step chemical route that has also been applied to synthesize other metal oxides, such as CuO,[11] α-Fe_2O_3,[12] γ-Al_2O_3,[13] and so on. Firstly, InOOH nanotubes and nanorods were synthesized by a solvothermal procedure in PEG-400. The shape and composition of the as-obtained products could be controlled by adjusting the amount of water and type of solvent used in the solvothermal process. Next, the transformation from InOOH to H-In_2O_3 was realized by thermal dehydration of the as-prepared InOOH nanocrystals in a tube furnace. The *in situ* release of H_2O from the oxyhydroxide materials during the decomposition process would retain the morphology of their oxyhydroxide precursors. As expected, the desired H-In_2O_3 nanotubes and nanorods were obtained.

Department of Chemistry, University of Science and Technology of China, Hefei, Anhui 230026, P. R. China. E-mail: zzd@ustc.edu.cn; Fax: +86 551 3601592; Tel: +86 551 3607752

† Electronic supplementary information (ESI) available: Further FT-IR spectra, TEM images and RhB solution photographs. See DOI: 10.1039/b817588h

Tubular and rod-like H-In_2O_3 nanocrystals are expected to find applications because their material properties are determined by structure, including size, morphology, pores, defects and composition.[14] Photocatalysis, with a primary focus on photocatalyst semiconductors such as TiO_2 and ZnO, is widely considered as an emerging technology for solving environmental problems; in particular, for the removal of organic contaminants.[15] As an important wide band gap semiconductor, cubic phase In_2O_3 (C-In_2O_3) has been applied to improve the photocatalytic efficiency of other semiconductors,[16] and has also been used as photocatalyst alone.[17] In this study, tubular and rod-like H-In_2O_3 nanostructures exhibit photocatalysis for the degradation of rhodamine B (RhB).

Experimental

Chemicals

The reaction was accomplished in a commercial Teflon-lined autoclave of 22 mL capacity. Indium trichloride tetrahydrate ($InCl_3{\cdot}4H_2O$) and hexamethylene diamine (HMDA) were used as reactants. The solvents used in this study were PEG-200 and PEG-400. All reagents were purchased from the Shanghai Chemical Company and used without further purification.

Synthesis of tubular and rod-like InOOH nanocrystals

In a typical synthesis, 0.5 mmol $InCl_3{\cdot}4H_2O$ and 0.15 mL distilled water were added to a 100 mL conical flask. After forming a solution, 19 mL PEG-400 and 2 mmol HMDA were also placed in the flask. The resulting solution was transferred into a Teflon-lined autoclave after magnetic stirring for about 1 h. The reactor was maintained at 210 °C for 24 h and then allowed to cool naturally to room temperature. The white precipitate was separated by centrifugation, and washed successively with distilled water and absolute ethanol to remove the residues of impurities. The collected products were dried under vacuum at 50 °C for 4 h before further characterization. The white products obtained were divided into two parts; one was subjected directly to characterization and the other was submitted to the following thermal treatment.

Synthesis of tubular and rod-like H-In_2O_3 nanocrystals

The decomposition of InOOH was conducted in a tube furnace with a temperature controller. In a typical procedure, the pre-synthesized white sample was loaded into a quartz boat and annealed at 400 °C for 10 min under ambient pressure and then cooled down to room temperature naturally. The heat rate for the tube furnace was 10 °C min^{-1} until the furnace temperature reached 400 °C. The final pale yellow products were collected for subsequent characterization.

Sample characterization

The crystal phases of the as-prepared products were characterized using a Philips X'Pert SUPER powder X-ray diffractometer with Cu-K_α radiation (λ = 1.5418 Å). Morphological and structural analyses of the samples were carried out by TEM and HRTEM (JEOL 2010 high resolution transmission electron microscope; accelerating voltage 200 kV). Fourier transform infrared (FT-IR) spectrometry was performed on a Perkin-Elmer spectrophotometer at room temperature. Thermogravimetry (TG) and differential thermal analysis (DTA) measurements were performed using a Shimadzu TA-50WS analyzer at temperatures ranging from room temperature to 600 °C. UV-vis diffuse reflectance spectra were recorded using a Shimadzu DUV-3700 spectrophotometer. Nitrogen sorption isotherms were measured at 77 K using Micromeritics ASAP2000 equipment. The BET (Brunauer–Emmett–Teller) method was used for specific surface area calculations.

Photocatalytic activity testing

A common method for evaluating the tubular and rod-like H-In_2O_3 nanocrystals' photocatalytic activity was to examine the bleaching of an organic dye solution following UV light illumination using UV-vis spectroscopy. The reaction system, containing 100 mL of an RhB ethanol solution with an initial concentration of 1.0×10^{-5} mol L^{-1} and 25 mg of as-synthesized H-In_2O_3, was magnetically stirred in the dark to reach a uniform dispersity and adsorption equilibrium. A high pressure mercury lamp was placed 20 cm from the solution and samples were collected every 30 min to analyse the RhB degradation by UV-vis spectroscopy.

Results and discussion

Characterization of tubular and rod-like InOOH nanocrystals

As mentioned in the Experimental section, tubular and rod-like InOOH nanostructures were synthesized by a HMDA-assisted solution method with PEG-400 used as the solvent. X-Ray diffraction (XRD) was used to verify the crystal structures and phase purity of samples. A typical XRD pattern of the as-prepared product is shown in Fig. 1. These broadened diffraction peaks could be indexed as orthorhombic InOOH with the cell parameters a = 5.23 Å, b = 4.55 Å and c = 3.26 Å, which are in good agreement with values from the standard card (JCPDS no. 71-2283). Note that the identity of the first reflection peak at 2θ = 20.5° could not be established on the basis of the available literature. A similar diffraction peak was observed in a previous report.[7e]

Fig. 2 provides direct information about the size and typical morphologies of the as-synthesized InOOH samples, suggesting that the product exhibits tubular and rod-like

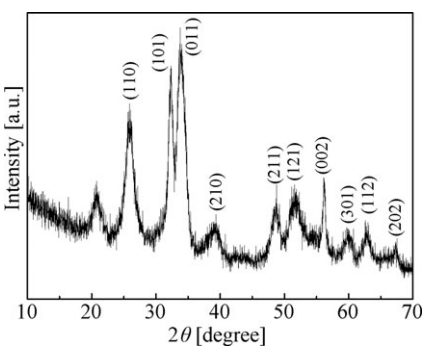

Fig. 1 The XRD pattern of tubular and rod-like InOOH nanostructures.

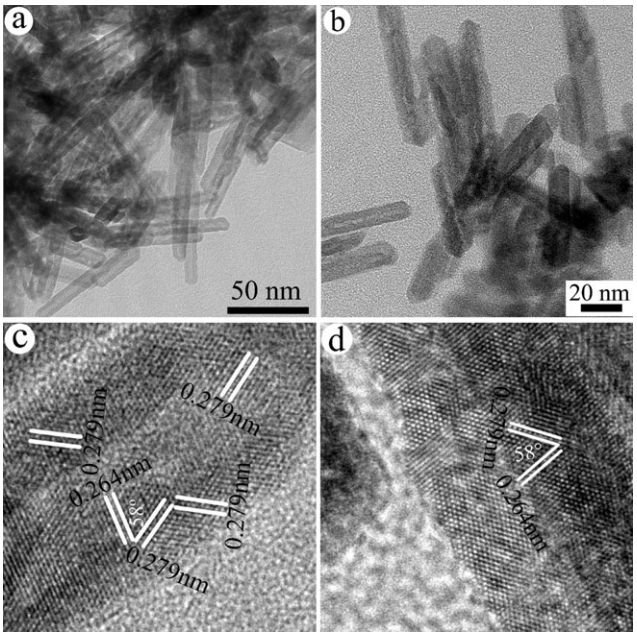

Fig. 2 Panoramic TEM images of the as-obtained InOOH (a) nanotubes, and (b) nanotubes and nanorods. HRTEM images of (c) a nanotube and (d) a nanorod.

nanostructures. Fig. 2a shows that the product is composed of InOOH nanotubes with closed tips. The tubular structure of the product is confirmed by the contrast between the dark edges and the pale centers. However, Fig. 2b reveals that the product obtained comprises both nanotubes and nanorods. The TEM image reveals InOOH 1-D nanostructures having lengths ranging from 30 to 60 nm and diameters in the range of 8–12 nm. The wall thickness of the nanotubes is in the range 2–3 nm. From these images, the statistical yield of tubular InOOH structures in the sample is about 45%. The corresponding high resolution transmission microscopy (HRTEM) images show that the nanotube (Fig. 2c) and nanorod (Fig. 2d) exhibit well-defined lattice fringes, indicating their single crystalline nature. There are two series of interplanar spacings in both HRTEM images. The marked two groups of crystal planes with interplanar spacings of 0.279 and 0.264 nm are the (101) and (200) planes of orthorhombic InOOH, respectively, and the calculated angle of 58.3° between the (101) and (200) planes is close to the measured angle of *ca.* 58°.

The growth mechanism of tubular and rod-like InOOH nanocrystals

To shed light on the formation mechanism of the final products, time-dependent experiments at various stages were followed by TEM, XRD and FT-IR during their growth processes.

Fig. 3 and Fig. 4 reveal the variation of the morphology and phase of the products prepared at various reaction stages. In the initial experiment, the aggregated nanoparticles and some short 1-D nanocrystals co-exist in the product after 0.5 h (Fig. 3a). XRD analyses (Fig. 4a) identify them as poorly-crystallized orthorhombic InOOH. It was clearly observed that 1-D nanocrystals gradually increase in quantity, and meanwhile the nanoparticles gradually decrease with

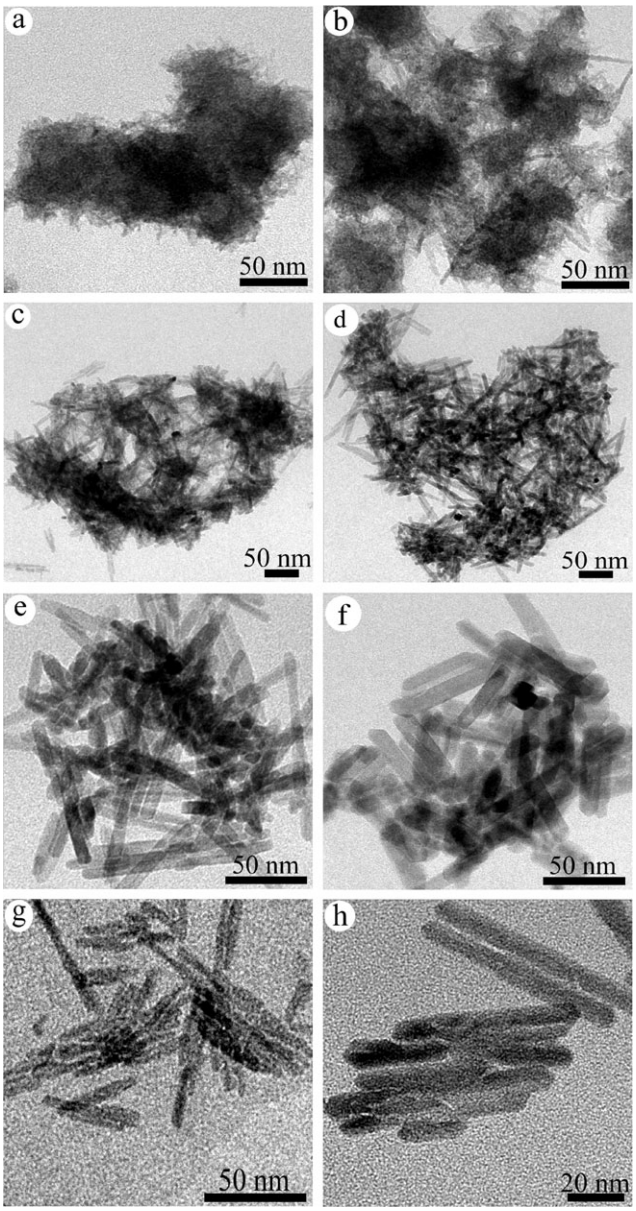

Fig. 3 Typical TEM images of InOOH samples after different reaction times: (a) 0.5 h, (b) 1 h, (c) 2 h, (d, g) 3 h, (e) 4 h and (f–h) 48 h.

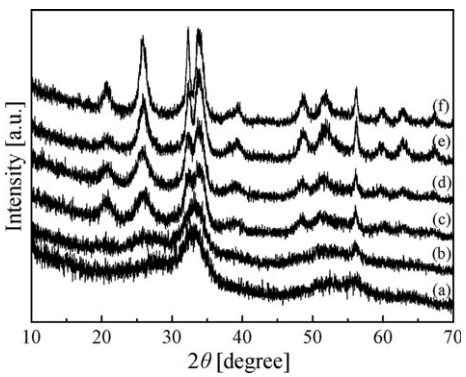

Fig. 4 (a–f) XRD patterns corresponding to samples prepared after reaction times from 1 to 48 h.

prolonged reaction time (Fig. 3, parts b and c). After a longer reaction time, the nanoparticles totally disappear, and a great many 1-D nanocrystals are obtained (Fig. 3, parts d and e). Correspondingly, the InOOH diffraction peaks gradually become sharper and stronger, as shown in Fig. 4, curves b–e. To reduce the overall high surface energy, the shape transformation from nanoparticles to 1-D nanostructures is driven by the coalescence of nanoparticles along certain preferential crystallographic directions of the orthorhombic InOOH.[18] Fig. 3f reveals that extending the reaction time beyond 24 h is unfavorable for the formation of uniform 1-D nanostructures in size. During the synthesis process, splitting rod-like structures can be observed (Fig. 3, parts g and h). Also, to explore the function of HMDA, samples obtained after different reaction times were closely monitored by FT-IR (ESI, Fig. S1†). Although most assignments in Fig. S1 are straightforward, some vibration peaks are different from pure HMDA molecules; the characteristic vibration peaks of the functional groups $–NH_2$ and $–CH_2–$ of the HMDA molecules are slightly shifted, which indicates that there is an interaction between the surfaces of the products and the HMDA molecules.

On the basis of above investigations, the formation of the tubular and rod-like InOOH nanostructures can be attributed to the HMDA molecule-assisted oriented attachment of nanoparticles and a dissolution–recrystallization process. These distinctive stages can be described sequentially. Initially, poorly-crystallized nanoparticles, stabilized by HMDA molecules, are yielded by the kinetically-driven hydrolysis of In^{3+}.[19] Upon extended heating, initially well-crystallized rod-shaped anisotropic nanostructures are yielded *via* the crystal-oriented attachment of pre-formed nanoparticles, with the assistance of surface-preferential HMDA adhesion, onto the lateral facets of the growing nanostructures, which reduces the overall surface energy by eliminating some of the high energy facets.[18] With the growth of rod-like InOOH structures, the concentration of H^+ ions gradually increases, corresponding to a decrease in the amount of reactants on the basis of the equation $In^{3+} + 2H_2O \rightarrow InOOH + 3H^+$, although H^+ ions can combine with alkalescence HMDA molecules to form an amine salt during the process. As ZnO nanotubes are obtained by the dissolution of ZnO nanowires in an acidic medium,[20] so the dissolution of pre-formed rod-like InOOH structures is initiated by the assistance of H^+ ions, and initially small-sized pores can be formed when the concentration of H^+ ions is high enough. TEM images of the final products, as shown in ESI, Fig. S2,† clearly reveal that there are many pores in the rod-like structures that are broken incompletely. These pores can be progressively conjoined by the dissolution of InOOH. Also, the dissolved In^{3+} ions can react with the OH^- ions obtained from the ionization of water to form InOOH, which recrystallizes onto the surface of the InOOH 1-D nanostructures due to its low solubility. Finally, InOOH nanorods and nanotubes co-exist in the final products.

Conditions for the formation of tubular and rod-like InOOH nanocrystals

In this work, to further uncover the optimal conditions for the formation of tubular and rod-like InOOH nanostructures, we carried out a set of experiments to investigate the effects of different parameters. From those experiments, we found that the amount of distilled water and the choice of solvent were key factors for the synthesis of high quality nanocrystals. In order to explore the role of PEG-400, PEG-200 was instead used as the solvent, and C-In_2O_3 with nanoflower-like structures was prepared (see Fig. 5, parts a and b). In a previous report, it was shown that In_2O_3 crystals can be directly obtained in diethylene glycol (DEG) based on the hydrolysis of indium alkoxide complexes at an elevated temperature.[21] Hence, PEG-200 could serve as a complexing agent and react with In^{3+} to form complexes that facilitate the formation of a cubic In_2O_3 phase. There could be a reaction between water and the complexes instead of the direct hydrolysis of In^{3+}. Fig. 5, parts c, e and f, reveal that the morphologies of the samples are sensitive to the amount of water. Interestingly, when the amount of water was reduced to 0.05 mL, the XRD pattern (Fig. 5d) proves that the product is not InOOH but C-In_2O_3, which can be ascribed to small amounts of water favoring the formation of complexes between In^{3+} and PEG-400. These results strongly suggest that InOOH 1-D nanostructures can only be obtained in distilled water within a narrow range (0.1–0.4 mL).

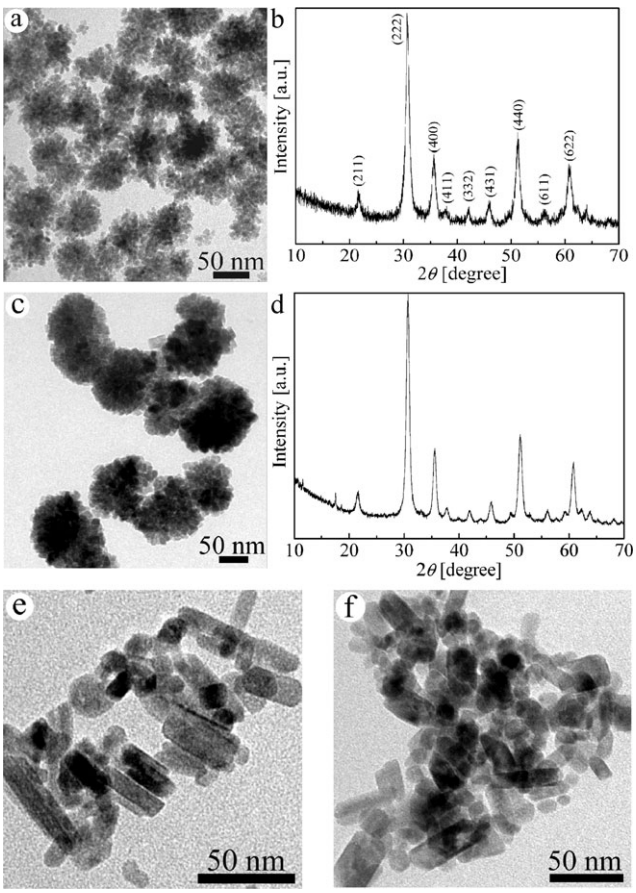

Fig. 5 TEM images of samples prepared under different conditions: (a) PEG-200 used as the solvent and V_{water} = 0.15 mL; (c) V_{water} = 0.05 mL, (e) V_{water} = 0.5 mL, and (f) V_{water} = 1.0 mL while PEG-400 used as solvent. XRD patterns (b) and (d) correspond to samples (a) and (c), respectively.

Characterization of tubular and rod-like H-In_2O_3 nanocrystals

After annealing the as-obtained InOOH precursors at 400 °C for 10 min under ambient pressure, H-In_2O_3 was prepared. The conversion process of the InOOH sample prepared by calcination in air was studied by TG and DTA (Fig. 6a). The TG curve can essentially be divided into two weight loss steps. The first step between 25 and 290 °C is mainly attributed to the desorption of HMDA molecules from the surface of the InOOH sample, which is consistent with the IR spectral data; the DTA curve indicates an endothermic process during this weight loss step. The second step between 290 and 425 °C, corresponding to an endothermic reaction, is ascribed to the chemical dehydration of InOOH ($2InOOH \rightarrow In_2O_3 + H_2O$); the weight loss of this step is about 6.4%, which agrees well with the amount of H_2O produced by the complete dehydration of stoichiometric InOOH. Fig. 6b shows the XRD pattern of the products obtained from the calcination of InOOH. All the diffraction peaks can be perfectly indexed to corundum-type In_2O_3 (JCPDS card no. 22-0336). No other impurities, such as InOOH or C-In_2O_3, were detected, which is indicative of a sample of high purity.

TEM images of H-In_2O_3, as shown in Fig. 7, were used to analyze the morphologies and structures of the as-synthesized sample. The panoramic observation (Fig. 7a) indicates that the annealed nanocrystals inherit well the morphology of their InOOH precursor, and consist of well shaped tubular and rod-like structures with lengths of 30–60 nm. The magnified TEM image (Fig. 7b) clearly reveals that the 1-D nanostructure is still retained, but its size has shrunken slightly due to the dehydration of InOOH during the calcination process, resulting in a high density. The corresponding HRTEM images (Fig. 7, parts c and d) of a typical annealed nanotube and nanorod exhibit well-defined lattice fringes, indicating their single crystalline nature. The interplanar spacing of 0.276 nm shown in both images corresponds to the (110) planes of hexagonal In_2O_3, which has an interplanar spacing of 0.274 nm.

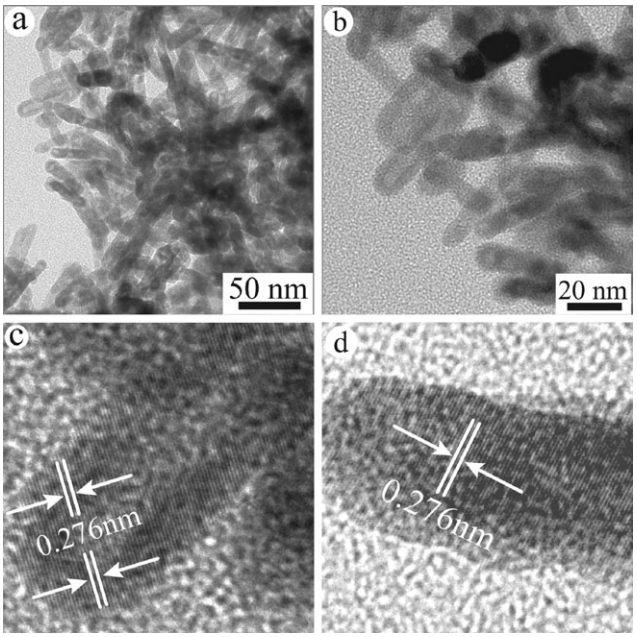

Fig. 7 TEM images of the as-obtained tubular and rod-like H-In_2O_3 structures: (a) panoramic morphology and (b) high magnification image. HRTEM images of an H-In_2O_3 (c) nanotube and (d) nanorod.

Optical properties of tubular and rod-like H-In_2O_3 nanocrystals

The UV-vis spectrum of as-synthesized H-In_2O_3 was recorded to investigate its optical properties, as shown in Fig. 8. The absorption spectrum of the H-In_2O_3 1-D nanocrystals shows a shoulder located at about 320 nm, corresponding to a band gap of 3.88 eV. The direct band gap of bulk In_2O_3 is known to be 3.75 eV, where the bottom of the conduction band is the In^{3+}-5s band and the top of the valence band is the O^{2-}-$2p^6$ band.[22] Compared with the band gap of bulk In_2O_3, the remarkable blue shift for the sample is probably attributable to the small dimensions of In_2O_3 nanocrystals.[23]

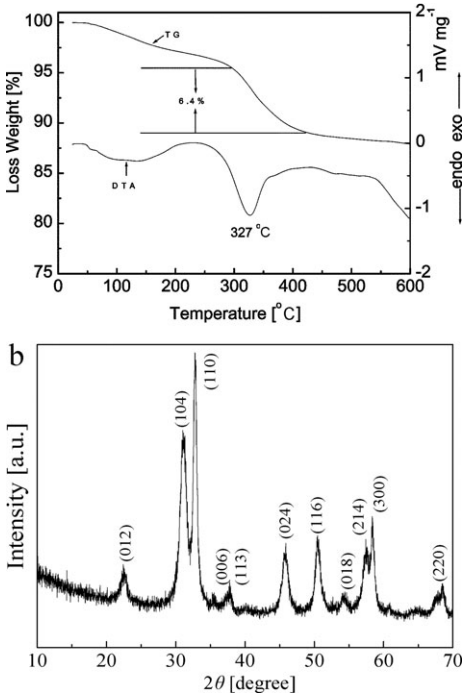

Fig. 6 (a) TG and DTA curves of the obtained InOOH. (b) XRD pattern of H-In_2O_3.

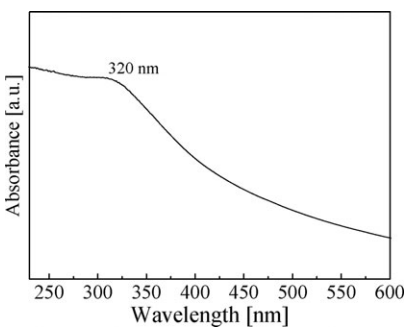

Fig. 8 The UV-vis spectrum of tubular and rod-like H-In_2O_3 structures.

Photocatalytic performance of tubular and rod-like H-In_2O_3 nanocrystals

To investigate the photocatalytic activity of the tubular and rod-like H-In_2O_3 nanocrystals in the degradation of organic pollutants, we carried out experiments of the photocatalytic degradation of rhodamine B (RhB). The UV-vis diffuse reflectance spectrum of the H-In_2O_3 1-D nanostructures implies the possibility of a high photocatalytic activity of the nanomaterials under UV light irradiation, carried out by using a high pressure mercury lamp with its wavelength concentrated at 254 nm. Under irradiation, the pink color of the RhB solution gradually faded (ESI, Fig. S3†). The temporal UV-vis spectral changes of the RhB solution during the photocatalytic degradation reactions are shown in Fig. 9a. The main absorbance, which was maximized at *ca.* 543 nm, decreased markedly with a prolonged irradiation time. These results indicate that RhB undergoes an obvious degradation under the catalysis of the tubular and rod-like H-In_2O_3 nanocrystals. To demonstrate the photocatalytic efficiencies of the tubular and rod-like H-In_2O_3 nanocrystals, we studied the photodegradation of RhB under different conditions, as shown in Fig. 9b. C is the absorption of the RhB solution at a wavelength of 543 nm after a particular irradiation time and C_0 is the absorption after absorption equilibrium on the surface of the photocatalyst before irradiation. The photodegradation efficiency is only 19% without any photocatalyst or exposure to UV light for 3 h (Fig. 9b, curve (1)), which indicates that the degradation of RhB is extremely slow under these conditions. Fig. 9b, curves (2) and (3) reveal that the degradation efficiency of different In_2O_3 structures is about 69 and 81%, respectively, when RhB/In_2O_3 suspensions were irradiated for 3 h. These experimental results reveal that tubular and rod-like H-In_2O_3 nanocrystals have superior photocatalytic activities over In_2O_3 nanocubes, which were also prepared on the basis of a literature report.[24] Generally, the photocatalytic behavior of semiconductors is mainly dependent on the separation of photogenerated electron–hole pairs[25] and the transfer of the separated electrons from the photocatalyst to the organic pollutant through oxygen vacancy defects on the surface of the photocatalyst.[26] In our study, oxygen vacancy defects can be generated during the transformation process from InOOH to In_2O_3 through heat treatment. The size and surface area of the photocatalyst play important roles in improving their photocatalytic performance.[27] Small size can reduce the recombination opportunities of electron–hole pairs. In addition, BET measurements show that the specific surface area of tubular and rod-like H-In_2O_3 nanostructures is 39.6 $m^2\ g^{-1}$, whereas that of In_2O_3 nanocubes is 21.2 $m^2\ g^{-1}$. The BET surface area increases with decreasing photocatalyst size, which is beneficial for absorbing more light and increasing the number of reaction sites. Hence, the as-synthesized H-In_2O_3 1-D nanocrystals have a good photocatalytic efficiency for RhB and are likely to be a good photocatalyst in applied fields.

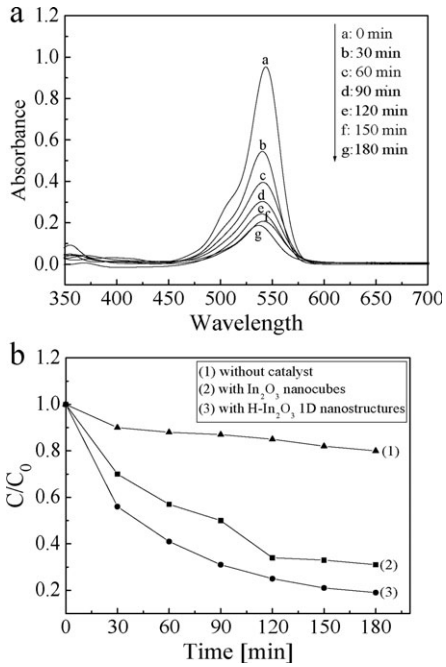

Fig. 9 (a) Absorption spectra of RhB solutions (5.0×10^{-5} mol L^{-1}, 100 mL) in the presence of 25 mg of tubular and rod-like H-In_2O_3 nanocrystals after exposure to UV light for different times. (b) A photocatalytic efficiency comparison under different conditions: (1) blank test, (2) with In_2O_3 nanocubes and (3) with tubular and rod-like H-In_2O_3 nanocrystals.

Conclusions

In conclusion, tubular and rod-like InOOH nanostructures were successfully synthesized by a simple and mild solvothermal method. The solvent, HMDA, and amount of water have significant effects on the formation of the phase and the shape of the final products. The anisotropic growth of InOOH can be attributed to HMDA molecule-assisted oriented attachment of nanoparticles, and the formation of tubular InOOH nanostructures may be due to "dissolution and recrystallization". As desired, tubular and rod-like H-In_2O_3 nanocrystals were obtained by the heat treatment of tubular and rod-like InOOH nanostructure precursors. It is still a challenge to prepare pure InOOH nanotubes, which is a target in our future research. The as-obtained tubular and rod-like H-In_2O_3 nanocrystals exhibited effective photocatalysis under UV light irradiation. The photocatalytic behavior of H-In_2O_3 is mainly dependent on photogenerated electron–hole pairs.

Acknowledgements

Financial support from the National Nature Science Research Foundation of China is gratefully acknowledged.

References

1 (*a*) A. Thiaville and J. Miltat, *Science*, 1997, **284**, 1939; (*b*) Y. Xia, P. Yang, Y. Sun, Y. Wu, B. Mayers, B. Gates, Y. Yin, F. Kim and H. Yan, *Adv. Mater.*, 2003, **15**, 353.
2 (*a*) S. Iijima, *Nature*, 1991, **354**, 56; (*b*) M. H. Huang, Y. Wu, H. Feick, N. Tran, E. Weber and P. Yang, *Adv. Mater.*, 2001, **13**, 113; (*c*) A. M. Morales and C. M. Lieber, *Science*, 1998, **279**, 208; (*d*) X. Wang and Y. Li, *J. Am. Chem. Soc.*, 2002, **124**, 2880; (*e*) Y. Xia, P. Yang, Y. Sun, Y. Wu, B. Mayers, B. Gates, Y. Yin, F. Kim and H. Yan, *Adv. Mater.*, 2003, **15**, 353; (*f*) H. Cölfen and

S. Mann, *Angew. Chem., Int. Ed.*, 2003, **42**, 2350; (*g*) X. W. Lou and H. C. Zeng, *J. Am. Chem. Soc.*, 2003, **125**, 2697.
3 (*a*) J. Hu, T. W. Odom and C. M. Lieber, *Acc. Chem. Res.*, 1999, **32**, 435; (*b*) X. Peng, L. Manna, W. Yang, J. Wickham, E. Scher, A. Kadavanich and A. P. Alivisatos, *Nature*, 2000, **404**, 59.
4 (*a*) T. Kijima, T. Yoshimura, M. Uota, T. Ikeda, D. Fujikawa, S. Mouri and S. Uoyama, *Angew. Chem., Int. Ed.*, 2004, **43**, 228; (*b*) P. Hoyer, *Langmuir*, 1996, **12**, 1411; (*c*) A. N. Aleshin, *Adv. Mater.*, 2006, **18**, 17; (*d*) S. Kobayashi, N. Hamasaki, M. Suzuki, M. Kimura, H. Shirai and K. Hanabusa, *J. Am. Chem. Soc.*, 2002, **124**, 6550.
5 (*a*) M. Kaempgen, M. Lebert, N. Nicoloso and S. Roth, *Appl. Phys. Lett.*, 2008, **92**, 094103; (*b*) T. Wang, X. Hu and S. Dong, *J. Mater. Chem.*, 2007, **17**, 4189; (*c*) L. Vayssieres, K. Keis, A. Hagfeldt and S.-E. Lindquist, *Chem. Mater.*, 2001, **13**, 4395; (*d*) X. Quan, S. Yang, X. Ruan and H. Zhao, *Environ. Sci. Technol.*, 2005, **39**, 3770; (*e*) Y. Huang, X. Duan, Q. Wei and C. M. Lieber, *Science*, 2001, **291**, 630; (*f*) O. K. Varghese, D. Gong, M. Paulose, K. G. Ong and C. A. Grimes, *Sens. Actuators, B*, 2003, **93**, 338; (*g*) O. K. Varghese, D. Gong, M. Paulose, K. G. Ong, E. C. Dickey and C. A. Grimes, *Adv. Mater.*, 2003, **15**, 624.
6 A. Gurlo, M. Ivanovskaya, N. Barsan, M. Schweizer-Berberich, U. Weimar, W. Gopel and A. Dieguez, *Sens. Actuators, B*, 1997, **44**, 327.
7 (*a*) Z. Zhuang, Q. Peng, J. Liu, X. Wang and Y. Li, *Inorg. Chem.*, 2007, **46**, 5179; (*b*) M. Epifani, P. Siciliano, A. Gurlo, N. Barasan and U. Weimar, *J. Am. Chem. Soc.*, 2004, **126**, 4078; (*c*) C. H. Lee, M. Kim, T. Kim, A. Kim, J. Paek, J. W. Lee, S.-Y. Choi, K. Kim, J.-B. Park and K. Lee, *J. Am. Chem. Soc.*, 2006, **128**, 9326; (*d*) J. Q. Xu, Y. P. Chen, Q. Y. Pan, Q. Xiang, Z. X. Cheng and X. W. Dong, *Nanotechnology*, 2007, **18**, 115615; (*e*) C. Chen, D. Chen, X. Jiao and C. Wang, *Chem. Commun.*, 2006, 4632; (*f*) D. Yu, S.-H. Yu, S. Zhang, J. Zuo, D. Wang and Y. Qian, *Adv. Funct. Mater.*, 2003, **13**, 497; (*g*) D. Chu, Y.-P. Zeng, D. Jiang and J. Xu, *Nanotechnology*, 2007, **18**, 435605.
8 C. Santato, M. Odziemkowski, M. Ulmann and J. Augustynski, *J. Am. Chem. Soc.*, 2001, **123**, 10639.
9 D. Zhang, H. Fu, L. Shi, C. Pan, Q. Li, Y. Chu and W. Yu, *Inorg. Chem.*, 2007, **47**, 2446.
10 F. Xu, Y. Xie, X. Zhang, C. Wu, W. Xi, J. Hong and X. Tian, *New J. Chem.*, 2003, **27**, 1331.
11 X. Zhang, G. Wang, X. Liu, J. Wu, M. Li, J. Gu, H. Liu and B. Fang, *J. Phys. Chem. C*, 2008, **112**, 16845.
12 X. Gou, G. Wang, X. Kong, D. Wexler, J. Horvat, J. Yang and J. Park, *Chem.–Eur. J.*, 2008, **14**, 5996.
13 L. Zhang and Y.-J. Zhu, *J. Phys. Chem. C*, 2008, **112**, 16764.
14 (*a*) Y. Zheng, L. Zheng, Y. Zhan, X. Lin, Q. Zheng and K. Wei, *Inorg. Chem.*, 2007, **46**, 6980; (*b*) C. Ye, Y. Bando, G. Shen and D. Golberg, *J. Phys. Chem. B*, 2006, **110**, 15146; (*c*) Y. Zheng, Y. Cheng, Y. Wang, F. Bao, L. Zhou, X. Wei, Y. Zhang and Q. Zheng, *J. Phys. Chem. B*, 2006, **110**, 3093; (*d*) Y. Zheng, C. Chen, Y. Zhan, X. Lin, Q. Zheng, K. Wei, J. Zhu and Y. Zhu, *Inorg. Chem.*, 2007, **46**, 6675.
15 (*a*) M. R. Hoffmann, S. T. Matin, W. Choi and D. W. Bahnemann, *Chem. Rev.*, 1995, **95**, 69; (*b*) A. Linsebigler, G. Lu and J. T. Yates, *Chem. Rev.*, 1995, **95**, 735.
16 (*a*) D. Shchukin, S. Poznyak, A. Kulak and P. Pichat, *J. Photochem. Photobiol., A*, 2004, **162**, 423; (*b*) S. K. Poznyak, D. V. Talapin and A. I. Kulak, *J.Phys. Chem. B*, 2001, **105**, 4816; (*c*) D. G. Shchukin and R. A. Caruso, *Chem. Mater.*, 2004, **16**, 2287; (*d*) X. Yang, Y. Wang, L. Xu, X. Yu and Y. Guo, *J. Phys. Chem. C*, 2008, **112**, 11481.
17 (*a*) S. K. Poznyak, A. N. Golubev and A. I. Kulak, *Surf. Sci.*, 2000, **454–456**, 396; (*b*) B. Li, Y. Xie, M. Jing, G. Rong, Y. Tang and G. Zhang, *Langmuir*, 2006, **22**, 9380.
18 (*a*) P. D. Cozzoli, T. Pellegrino and L. Manna, *Chem. Soc. Rev.*, 2006, **35**, 1195; (*b*) Y.-W. Jun, J.-S. Choi and J. Cheon, *Angew. Chem., Int. Ed.*, 2006, **45**, 3414.
19 H. Zhang, Q. Zhu, Y. Zhang, Y. Wang, L. Zhao and B. Yu, *Adv. Funct. Mater.*, 2007, **17**, 2766.
20 C. Yan and D. Xue, *Electrochem. Commun.*, 2007, **7**, 1247.
21 J. Yang, C. Li, Z. Quan, D. Kong, X. Zhang, P. Yang and J. Lin, *Cryst. Growth Des.*, 2007, **8**, 695.
22 (*a*) S. J. Wen, G. Campet, J. Portier, G. Couturier and J. B. Goodenough, *Mater. Sci. Eng., B*, 1992, **14**, 115; (*b*) I. Hamberg and C. G. Granqvist, *Sol. Energy Mater. Sol. Cells*, 1986, **14**, 241.
23 R. B. H. Tahar, T. Ban, Y. Ohya and Y. Takahashi, *J. Appl. Phys.*, 1997, **82**, 865.
24 L.-Y. Chen, Y.-G. Zhang, W.-Z. Wang and Z.-D. Zhang, *Eur. J. Inorg. Chem.*, 2008, 1445.
25 A. Kudo, K. Omori and H. Kato, *J. Am. Chem. Soc.*, 1999, **121**, 11459.
26 Y. Zheng, C. Chen, Y. Zhan, X. Lin, Q. Zheng, K. Wei and J. Zhu, *J. Phys. Chem. C*, 2008, **112**, 10773.
27 M. Shang, W. Wang, S. Sun, L. Zhou and L. Zhang, *J. Phys. Chem. C*, 2008, **112**, 10407.